

The “Yin-Yang Grid”: An Overset Grid in Spherical Geometry

Akira Kageyama* and Tetsuya Sato

Earth Simulator Center, Japan Agency for Marine-Earth Science and Technology, Yokohama 236-0001, Japan

A new kind of overset grid, named Yin-Yang grid, for spherical geometry is proposed. The Yin-Yang grid is composed of two identical component grids that are combined in a complementary way to cover a spherical surface with partial overlap on their boundaries. Each component grid is a low latitude part of the latitude-longitude grid. Therefore the grid spacing is quasi-uniform and the metric tensors are simple and analytically known. One can directly apply mathematical and numerical resources that have been written in the spherical polar coordinates or latitude-longitude grid. The complementary combination of the two identical component grids enables us to make efficient and concise programs. Simulation codes for geodynamo and mantle convection simulations using finite difference scheme based on the Yin-Yang grid are developed and tested. The Yin-Yang grid is suitable for massively parallel computers.

I. INTRODUCTION

Since the Earth is composed of spherical layers, computer simulations of the Earth’s interior, such as geodynamo and mantle convection simulations, need efficient spatial discretization schemes in spherical shell geometry. The spectral method [15] has been the major tool in the geodynamo simulation; all six codes [9, 11, 42, 46, 47] in the benchmark test in *Christensen et al.* [10] and other codes [e.g., 20, 28] use the spherical harmonics expansion method in the horizontal space. However, the importance of non-spectral (or point-based) approaches in the dynamo simulation is now increasingly recognized to simulate more realistic geodynamo regime with smaller Ekman numbers [7]. The pursuit of point-based approaches started earlier in the mantle convection simulations, because the mantle’s intense spatial variation of viscosity and the phase transitions makes the spectral approach not fit to the problem. Although the spectral method for the mantle convection prospered in 1980s and 90s [2, 16, 18, 30, 49], the finite element method is rapidly growing in this field [1, 4, 39, 45, 50]. There are also a couple of codes that uses the finite element method in the geodynamo simulation [7, 31]. The finite difference or finite volume method is applied for the mantle convection by *Hernlund and Tackley* [19], *Iwase* [21], *Ratcliff et al.* [38]. The finite difference method has been used for the core convection and the geodynamo simulation by the authors from 1990s [22, 23, 24, 25, 26, 27, 29, 34], in which the latitude-longitude grids in the spherical polar coordinates is used with radius r ($r_i \leq r \leq r_o$), colatitude θ ($0 \leq \theta \leq \pi$), and longitude ϕ ($0 \leq \phi < 2\pi$). Since the finite difference method enables us to make highly optimized programs for massively parallel computers, especially massively parallel vector supercomputers like the Earth Simulator [17], we further exploit the possibility of the finite difference method for simulations in spherical shell geometry by improving the base grid system.

It is known that the latitude-longitude grid has two numerical problems; the coordinate singularity and the grid convergence near the poles. Since the coordinate singularity is not a real singularity (the pole is not singular point of physical functions), one can solve the basic equations on the poles by applying the l’Hospital’s rule on the pole grids [e.g., 26]. The computational cost for this pole grid solver is negligible.

The problem of the grid convergence is more serious. In order to relax the severe restriction on the time step, one has to apply a filter so that the grid spacing on the sphere becomes *effectively* quasi-uniform. The amount of information abandoned by the filter is estimated by the number of grid points that are *effectively* present and that *actually* present in the computational space; suppose one has a latitude-longitude grid of a spherical surface of unit radius with inter mesh angles Δ in both colatitude (θ) and longitude (ϕ). The azimuthal grid spacing, which is Δ in the equator, converges in higher latitudes. When a filter enables an effectively quasi-uniform grid with spacing Δ on the sphere, the number of effective grid points is estimated by $(\int_0^\pi \sin \theta d\theta \int_0^{2\pi} d\phi) / \Delta^2 = 4\pi / \Delta^2$. While the number of actual grid points in the computational space is given by $(\int_0^\pi d\theta \times \int_0^{2\pi} d\phi) / \Delta^2 = 2\pi^2 / \Delta^2$. Therefore sizeable ratio of information, $(2\pi^2 - 4\pi) / 2\pi^2 \sim 36\%$ of the latitude-longitude grid, is abandoned in vain by the filtering at each simulation step. In addition to this computational inefficiency, the filter has non-negligible computational costs. In our geodynamo simulation code using latitude-longitude grid, in which a Fast Fourier Transform (FFT)-based filtering procedure is applied, the filter routine can take more than 30% of the total execution time.

*Electronic address: kage@jamstec.go.jp

Note that the above problem of the grid redundancy in the latitude-longitude grid comes only from the region of high latitudes. The remaining part of the latitude-longitude grid—the low latitude region—has rather desirable feature for numerical simulations; it is an orthogonal grid, it has simple metric tensors, and it has quasi-uniform grid spacings. This observation leads us to the idea of a new spherical grid proposed in this paper.

Since there is no grid mesh that is orthogonal all over the spherical surface and, at the same time, free of coordinate singularity or grid convergence, we decompose the spherical surface into subregions. The decomposition, or dissection, enables us to cover each subregion by a grid system that is individually orthogonal and singularity-free. This *divide-and-rule* approach has been used with good success in the computational aerodynamics that incorporates complex geometry of aircraft's body with wings/stores/blades.

The dissection of the computational domain generates internal border or boundary between the subregions. There are two different approaches to handle the internal boundaries. One is the patched grid method [37] and the other is the overset grid method [8]. In the patched grid approach, the subdomains contact one another without any overlap on their borders. In the overset grid method, on the other hand, the subdomains partially overlap one another on their borders. The overset grid is also called as overlaid grid, or composite overlapping grid, or Chimera grid [44]. The validity and importance of the overset approach in the aerodynamical calculations was pointed out by *Steger* [43]. Since then this method is widely used in this field. It is now one of the most important grid techniques in the computational aerodynamics; for example, whole aircraft with wing and store [32], tiltrotor aircraft [33], Boeing 747 [6, 40], Space Shuttle [5], helicopter [13], and others.

In the computational geosciences, the idea of the overset grid approach appeared rather early. *Phillips* proposed a kind of composite grid in 1950's to solve partial differential equations on a hemisphere, in which the high latitude region of the latitude-longitude grid is “capped” by another grid system that is constructed by a stereographic projection to a plane on the north pole [3, 35, 36]. After a long intermission, the overset grid method seems to attract growing interest in geoscience these days. The “cubed sphere” [41] is an overset grid that covers a spherical surface with six component grids that correspond to six faces of a sphere. The “cubed sphere” is recently applied to the mantle convection simulation [19]. In the atmospheric research, other kind of spherical overset grid is used in a global circulation model [12], in which the spherical surface is covered by two component grids—improved stereographic projection grids—in northern and southern hemispheres that overlap in the equator. A successful test of 100-day integration of global circulation is demonstrated with this overset grid.

The overset grid proposed in this paper is named “Yin-Yang grid” after the symbol for yin and yang of Chinese philosophy of complementarity. The Yin-Yang grid is composed of two identical and complementary component grids. Compared with other spherical overset grids, the Yin-Yang grid is simple in its geometry and metric tensors. A remarkable feature of this overset grid is that the two identical component grids are combined in a complementary way with a special symmetry.

II. BASIC YIN-YANG GRID

The Yin-Yang grid in its most basic shape is shown in Fig. 1. It has two component grids that are geometrically identical (exactly the same shape and size); see Fig. 1(a). We call the two component grids “Yin grid” (or n -grid) and “Yang grid” (or e -grid). They are combined to cover a spherical surface with partial overlap on their borders as shown in Fig. 1(b). Each component grid is in fact a part of the latitude-longitude grid: A component grid, say Yin grid, is defined in the spherical polar coordinates by

$$(\pi/4 - \delta \leq \theta \leq 3\pi/4 + \delta) \cap (-3\pi/4 - \delta \leq \phi \leq 3\pi/4 + \delta), \quad (1)$$

where δ is a small buffer, which is proportional to grid spacing, required for minimum overlap in the overset methodology (see Fig. 1(b)). In the limit of infinitesimal grid ($\delta \rightarrow 0$), the area of the above part of the sphere with unit radius is given by $\int_{\pi/4}^{3\pi/4} \sin\theta d\theta \int_{-3\pi/4}^{3\pi/4} d\phi = 3\pi/\sqrt{2} \sim 2.12\pi$, i.e., roughly a half of the whole spherical surface (2π). Another component grid, Yang grid, is defined by the same rule of eq. (1) but in different spherical coordinates that is perpendicular to the original one; see the green- and blue-colored spherical mesh in Fig. 2. The axis of the Yang grid's coordinates (blue mesh in Fig. 2), is located in a equator of the Yin grid's coordinates (green mesh in Fig. 2). The relation between Yin coordinates and Yang coordinates is denoted in the Cartesian coordinates by

$$(x^e, y^e, z^e) = (-x^n, z^n, y^n), \quad (2)$$

where (x^n, y^n, z^n) is Yin's Cartesian coordinates and (x^e, y^e, z^e) is Yang's. In a matrix form,

$$\begin{pmatrix} x^e \\ y^e \\ z^e \end{pmatrix} = M \begin{pmatrix} x^n \\ z^n \\ y^n \end{pmatrix}, \quad (3)$$

where

$$M = \begin{pmatrix} -1 & 0 & 0 \\ 0 & 0 & 1 \\ 0 & 1 & 0 \end{pmatrix}. \quad (4)$$

Note that

$$M^{-1} = M, \quad (5)$$

which indicates that the transformations between Yin and Yang coordinates are symmetric. This is a reflex of the complementary relation between Yin and Yang.

In the spherical coordinates, eq. (2) reads

$$r^e = r^n, \quad (6)$$

$$\sin \theta^e \cos \phi^e = -\sin \theta^n \cos \phi^n, \quad (7)$$

$$\sin \theta^e \sin \phi^e = \cos \theta^n, \quad (8)$$

$$\cos \theta^e = \sin \theta^n \sin \phi^n, \quad (9)$$

where (r^n, θ^n, ϕ^n) , and (r^e, θ^e, ϕ^e) are the coordinates of Yin and Yang, respectively. The idea of two perpendicular spherical coordinates is used in the global ocean simulation [14] to avoid the grid convergence in the Arctic, however, the second spherical coordinates is used in a sort of auxiliary way for the main (usual) spherical polar coordinates in their method. On the other hand, we make the best use of the symmetry between two coordinates.

For spatial discretization, we define mesh point at j -th colatitude θ_j^ℓ and k -th longitude ϕ_k^ℓ on Yin grid (for $\ell = n$) and on Yang grid (for $\ell = e$) as

$$\theta_j^\ell = \theta_{\min} + j \Delta\theta, \quad (j = 0, N_\theta - 1), \quad (10)$$

$$\phi_k^\ell = \phi_{\min} + k \Delta\phi, \quad (k = 0, N_\phi - 1), \quad (11)$$

with

$$\Delta\theta = (\theta_{\max} - \theta_{\min}) / (N_\theta - 1), \quad (12)$$

$$\Delta\phi = (\phi_{\max} - \phi_{\min}) / (N_\phi - 1), \quad (13)$$

where the grid distribution ranges from $\theta_{\min} = \pi/4 - \delta$ to $\theta_{\max} = 3\pi/4 + \delta$ in colatitude, and from $\phi_{\min} = -3\pi/4 - \delta$ to $\phi_{\max} = 3\pi/4 + \delta$ in longitude. We set $\Delta\theta = \Delta\phi = 2\delta$ in Fig. 1, as an example.

An important feature of the Yin-Yang grid as a spherical overset grid is that the two component grids are identical and their geometrical positions are complementary. This enables us to make concise programs: Suppose a grid point (θ_j^n, ϕ_k^n) on Yin grid's horizontal border at index position (j, k) (e.g., $j = 1$). Its value should be determined by an interpolation from its neighbor points, or stencils, of Yang grid with interpolation coefficients that are determined by relative position of (θ_j^n, ϕ_k^n) in the stencils. Note that exactly the same interpolation coefficients and relative stencils are used to set the value of corresponding grid point (θ_j^e, ϕ_k^e) at (j, k) of Yang's border, since the geometrical relations between Yin grid and Yang grid are symmetric. In other words, we can make use of one interpolation routine for two times (for Yin grid and for Yang grid) to set the horizontal boundary conditions. Note also that the metric tensors at a bulk grid point at (j, k) of Yin grid is a function of its position (θ_j^n, ϕ_k^n) in Yin's coordinates, and the metric tensors at corresponding point (θ_j^e, ϕ_k^e) in Yang grid are exactly the same. Therefore we can call one subroutine of fluid solver and others for two times for Yin grid and Yang grid.

Another advantage of the Yin-Yang grid resides in the fact that the component grid is nothing but the (part of) latitude-longitude grid. We can directly deal with the equations to be solved with the vector form in the usual spherical polar coordinates, $\{v_r, v_\theta, v_\phi\}$. The analytical form of metric tensors are familiar in the spherical coordinates. We can directly code the basic equations in the program as they are formulated in the spherical coordinates. We can make use of various resources of mathematical formulas, program libraries, and tools that have been developed in the spherical polar coordinates.

To conclude this section, we point out that the construction of three-dimensional Yin-Yang grid for spherical shell geometry is straightforward, by piling up the basic (two-dimensional) Yin-Yang grids in radial direction. See Fig. 3.

III. VECTOR TRANSFORMATION FORMULA BETWEEN YIN AND YANG GRIDS

Following the general overset methodology [e.g., 8], interpolations are applied on the boundary of each component grid to set the boundary values, or internal boundary condition. When one deals with scalar variables, the interpolation

is simple. For vector fields, a care is needed for vector components, since expressions of a vector in the Yin's spherical coordinates, $\{v_r^n, v_\theta^n, v_\phi^n\}$, and in the Yang's coordinates, $\{v_r^e, v_\theta^e, v_\phi^e\}$, are different.

Because the Yin-Yang transformation denoted by eq. (2) is a rotation about the origin ($r = 0$), the radial component of the vector is invariant ($v_r^n = v_r^e$), and horizontal components are mapped by local rotation transforms, as shown in Fig. 4, where the rotation angle ψ is a function of latitude and longitude;

$$\begin{pmatrix} v_r^e \\ v_\theta^e \\ v_\phi^e \end{pmatrix} = \begin{pmatrix} 1 & 0 & 0 \\ 0 & \cos \psi & -\sin \psi \\ 0 & \sin \psi & \cos \psi \end{pmatrix} \begin{pmatrix} v_r^n \\ v_\theta^n \\ v_\phi^n \end{pmatrix}. \quad (14)$$

To find the expression of ψ , we consider unit vectors in θ and ϕ directions on the Yin and Yang coordinates. From Fig. 4, we see

$$\cos \psi = \hat{\phi}^n \cdot \hat{\phi}^e, \quad (15)$$

$$\sin \psi = -\hat{\phi}^n \cdot \hat{\theta}^e, \quad (16)$$

where $\hat{\theta}^\ell$ and $\hat{\phi}^\ell$ are unit vectors in θ and ϕ directions in the component grid ℓ , with $\ell = n$ for Yin grid, and $\ell = e$ for Yang grid. The unit vectors $\{\hat{x}^\ell, \hat{y}^\ell, \hat{z}^\ell\}$ in the Cartesian coordinates are related to $\{\hat{\theta}^\ell, \hat{\phi}^\ell\}$ by

$$\hat{\phi}^e = -\sin \phi^e \hat{x}^e + \cos \phi^e \hat{y}^e, \quad (17)$$

$$\begin{aligned} \hat{\phi}^n &= -\sin \phi^n \hat{x}^n + \cos \phi^n \hat{y}^n \\ &= \sin \phi^n \hat{x}^e + \cos \phi^n \hat{z}^e, \end{aligned} \quad (18)$$

$$\hat{\theta}^e = \cos \theta^e \cos \phi^e \hat{x}^e + \cos \theta^e \sin \phi^e \hat{y}^e - \sin \theta^e \hat{z}^e. \quad (19)$$

Substituting eqs. (17) and (18) into (15), we get

$$\cos \psi = -\sin \phi^e \sin \phi^n. \quad (20)$$

Substituting eqs. (18) and (19) into (16), we get

$$\begin{aligned} \sin \psi &= \cos \theta^e \cos \phi^e \sin \phi^n - \sin \theta^e \cos \phi^n \\ &= \frac{1}{\sin \theta^e \sin \theta^n} \{ \cos \theta^e (\sin \theta^e \cos \phi^e) (\sin \theta^n \sin \phi^n) - \sin^2 \theta^e (\sin \theta^n \cos \phi^n) \} \\ &= -\frac{\cos \phi^e}{\sin \theta^n} \\ &= \frac{\cos \phi^n}{\sin \theta^e}. \end{aligned} \quad (21)$$

Here we have used eqs. (7)–(9).

From eqs. (20), (21), (15), (16) and (14), we obtain the transformation formula of the vector components (v_r, v_θ, v_ϕ) by

$$\begin{pmatrix} v_r^e \\ v_\theta^e \\ v_\phi^e \end{pmatrix} = P \begin{pmatrix} v_r^n \\ v_\theta^n \\ v_\phi^n \end{pmatrix}, \quad (22)$$

with the transformation matrix

$$P = \begin{pmatrix} 1 & 0 & 0 \\ 0 & -\sin \phi^e \sin \phi^n & -\cos \phi^n / \sin \theta^e \\ 0 & \cos \phi^n / \sin \theta^e & -\sin \phi^e \sin \phi^n \end{pmatrix}. \quad (23)$$

Since Yin and Yang coordinates are symmetric, the inverse transformation from Yang into Yin is given by the interchange of the suffixes:

$$P^{-1} = \begin{pmatrix} 1 & 0 & 0 \\ 0 & -\sin \phi^n \sin \phi^e & -\cos \phi^e / \sin \theta^n \\ 0 & \cos \phi^e / \sin \theta^n & -\sin \phi^n \sin \phi^e \end{pmatrix}. \quad (24)$$

Note also that

$$P^2 = 1, \quad (25)$$

which indicates the complementary relation between Yin and Yang coordinates.

When we see the component grid of the basic Yin-Yang grid shown in Fig. 1 in the Mercator projection, it is a rectangle; the four corners intrude most into the other component grid (see Fig. 1(b)). Even if the grid mesh is taken to be infinitesimal, i.e., $\Delta\theta = \Delta\phi \rightarrow 0$ and $\delta \rightarrow 0$, the overlapping area has still non-zero ratio of about 6%; $(3/\sqrt{2}\pi - 2\pi)/2\pi \sim 0.061$. This overlapped area can be minimized by modifying the component grid's shape from the rectangle. It is obvious that a Yin-Yang grid with minimum overlap region can be constructed by a division, or dissection, with a closed curve on a sphere that cuts the sphere into two identical parts. There are infinite number of such dissections of a sphere. Fig. 5 shows two examples among them. When we cut along the curve that is colored with red and blue in Fig. 5(a) or (b), we get two separated parts of the spherical surface that are identical. Although, it is not apparent that the two parts separated by the blue-red curve in each panel of Fig. 5 are identical from this figure, the corresponding three-dimensional view (Fig. 6) would show more convincingly. The cutoff curve of Fig. 6(a) reminds us a baseball, while the cutoff curve of Fig. 6(b) resembles a cube.

Based on these spherical dissections, we can construct spherical overset grids with two identical component grids that has minimum overlapping area; Fig. 7 shows a Yin-Yang grid that corresponds to the baseball type dissection of a sphere (panels labeled (a) in Figs. 5 and 6). Fig. 8 is for the cube type dissection (panels (b) of Figs. 5 and 6). When minimizing the computational cost is strongly required, the Yin-Yang grid of the baseball type (Fig. 7) or cube type (Fig. 8) would be worth trying.

However, the non-rectangle geometries of the component grid of Fig. 7 or Fig. 8 imply that special cares should be taken to mask some grid points. The number of the mask is the same for both the Yin-Yang grids of Figs. 7 and 8, since the non-masked area of a component grid is just a half of the spherical surface (2π) in the limit of the negligibly small overlap area.

IV. SUMMARY

For numerical simulations of the Earth's interior, we have developed a new spherical grid based on the overset grid methodology. Our motivation is to devise a spherical grid system that is suitable for finite difference scheme on massively parallel vector supercomputers. The spherical overset grid proposed in this paper, named Yin-Yang grid, is composed of two component grids. They have the same shape and size and combined to cover a spherical surface with partial overlap on their borders. Each component grid is nothing but low latitude region of the usual latitude-longitude grid; it is 90° about the equator and 270° in the longitude. Therefore the grid spacing is quasi-uniform and the metric tensors are simple and analytically known. One can directly apply mathematical and numerical resources that have been written in the spherical polar coordinates or latitude-longitude grid system. Since the two component grids are identical and combined in a complementary way, various routines for solvers and interpolation can be recycled for two times for each component grid at every simulation time step.

We have developed finite difference codes of the mantle convection and dynamo simulation using the basic Yin-Yang grid for spherical shell geometry (see Figs. 1 and 3). We have confirmed that the Yin-Yang grid is successfully applied to both cases. The mantle convection code is newly developed from scratch. Details of the code and simulation results are reported in other paper [48]; we solved the time development of thermal convection motion in a spherical shell of a Boussinesq fluid with infinite Prandtl number for uniform and variable viscosity cases. We have performed standard benchmark tests of the mantle convection [39], and confirmed that the results of our Yin-Yang mantle convection code successfully reproduced previously published results. The numerical values of Nusselt number and the mean velocity coincides with other benchmark values within a few percent or even better [48]. We have also applied the Yin-Yang grid to the geodynamo simulation code. The magnetohydrodynamic (MHD) equations with finite viscosity, thermal diffusivity, and electrical conductivity are solved. The Yin-Yang geodynamo code has been converted from our previous geodynamo code which was based on the latitude-longitude grid. We found that the code conversion was straightforward and rather easy since the base grid is common. We could reproduce our previous (latitude-longitude grid based) results of geodynamo simulation by our newly developed Yin-Yang geodynamo code with shorter calculation time. The details of the code will be reported in other paper.

The Yin-Yang grid is suitable for parallel programming. Since the number of the component grid is two, we are naturally lead to make parallel programs with domain decomposition of even number: We first decompose whole computational region into two—Yin component and Yang component—then apply further domain decomposition in each component.

Finally, we point out another possible spherical overset grid that has an odd number of component grids. Fig. 9 shows a spherical overset grid that consists of three identical component grids. In this case, the component grid is

defined as a part (about 1/3) of the spherical surface by $(\pi/4 \leq \theta \leq 3\pi/4) \cap (-\pi/2 \leq \phi \leq \pi/2)$. This grid could be effective when the processor number is multiple of three.

Acknowledgments

We would like to acknowledge helpful discussion with: Masanori Kameyama, Kenji Komine, Hideaki Miura, Keiko Takahashi, and Masaki Yoshida. The development and benchmark test of the mantle convection code using the Yin-Yang grid was done by Masaki Yoshida. All simulations were performed by Earth Simulator, Japan Agency for Marine-Earth Science and Technology.

-
- [1] Baumgardner, J. (1985), Three-dimensional treatment of convective flow in the earth's mantle, *J. Statist. Phys.*, *39*, 501–511.
 - [2] Bercovici, D., G. Schubert, G. A. Glatzmaier, and A. Zebib (1989), Three dimensional thermal convection in a spherical shell, *J. Fluid Mech.*, *206*, 75–104.
 - [3] Browning, G. L., J. J. Hack, and P. N. Swartrauber (1989), A comparison of three numerical methods for solving differential equations on the sphere, *Month. Weath. Rev.*, *117*, 1058–1075.
 - [4] Bunge, H.-P., and J. R. Baumgardner (1995), Mantle convection modeling on parallel virtual machines, *Comput. Phys.*, *9*, 207–215.
 - [5] Buning, P. G., I. T. Chiu, S. Obayashi, Y. M. Rizk, and J. L. Steger (1988), Numerical simulation of the integrated space shuttle vehicle in ascent, *AIAA Paper*, *88-4359-Cp*, 265–283.
 - [6] Cao, H. V., T. Y. Su, and S. E. Rogers (1998), Navier-stokes analysis of a 747 high lift configuration, *AIAA*, *98-2623*, 402–409.
 - [7] Chan, K. H., K. Zhang, J. Zou, and G. Schubert (2001), A non-linear, 3-D spherical α^2 dynamo using a finite element method, *Phys. Earth Planet. Inter.*, *128*, 35–50.
 - [8] Chesshire, G., and W. D. Henshaw (1990), Composite overlapping meshes for the solution of partial differential equations, *J. Comput. Phys.*, *90*, 1–64.
 - [9] Christensen, U., P. Olson, and G. A. Glatzmaier (1999), Numerical modelling of the geodynamo: a systematic parameter study, *Geophys. J. Int.*, *138*, 393–409.
 - [10] Christensen, U. R., et al. (2001), A numerical dynamo benchmark, *Physics of the Earth and Planetary Interiors*, *128*, 25–34.
 - [11] Dorny, E., P. Cardin, and D. Jault (1998), MHD flow in a slightly differentially rotating spherical shell, with conducting inner core, in a dipolar magnetic field, *Earth Planet. Sci. Lett.*, *160*, 15–30.
 - [12] Dudhia, J., and J. F. Bresch (2002), A global version of the PSU-NCAR mesoscale model, *Month. Weather Rev.*, *130*, 2989–3007.
 - [13] Duque, E. P. N., R. C. Strawn, J. Ahmad, and R. Biswas (1996), An overset grid navier-stokes kirchhoff-surface method for rotorcraft aeroacoustic predictions, *AIAA*, *96-0152*, 1–13.
 - [14] Eby, M., and G. Holloway (1994), Grid transformation for incorporating the Arctic in a global ocean model, *Climate Dynamics*, *10*, 241–247.
 - [15] Glatzmaier, G. (1984), Numerical simulations of stellar convective dynamos. I. the model and method, *J. Comput. Phys.*, *55*, 461–484.
 - [16] Glatzmaier, G. (1988), Numerical simulations of mantle convection: time-dependent, three-dimensional, compressible, spherical shell, *Geophys. Astrophys. Fluid Dyn.*, *43*, 223–264.
 - [17] Habata, S., M. Yokokawa, and S. Kitawaki (2003), The earth simulator system, *NEC Res. & Develop.*, *44*(1), 21–26.
 - [18] Harder, H., and U. R. Christensen (1996), A one-plume model of martian mantle convection, *Nature*, *380*, 507–509.
 - [19] Hernlund, J. W., and P. J. Tackley (2003), Three-dimensional spherical shell convection at infinite Prandtl number using the ‘cubed sphere’ method, *proceedings of the Second MIT Conference on Computational Fluid and Solid Mechanics*.
 - [20] Ishihara, N., and S. Kida (2002), Dynamo mechanism in a rotating spherical shell: Competition between magnetic field and convection vortices, *J. Fluid Mech.*, *465*, 1–32.
 - [21] Iwase, Y. (1996), Three-dimensional infinite Prandtl number convection in a spherical shell with temperature-dependent viscosity, *J. Geomag. Geoelectr.*, *48*, 1499–1514.
 - [22] Kageyama, A., and T. Sato (1997), Generation mechanism of a dipole field by a magnetohydrodynamic dynamo, *Phys. Rev. E*, *55*, 4617–4626.
 - [23] Kageyama, A., and T. Sato (1997), Velocity and magnetic field structures in a magnetohydrodynamic dynamo, *Phys. Plasmas*, *4*, 1569–1575.
 - [24] Kageyama, A., and T. Sato (1997), Dipole field generation by an MHD dynamo, *Plasma Phys. Contr. Fusion*, *39*, A83–A91.
 - [25] Kageyama, A., K. Watanabe, and T. Sato (1993), Simulation study of a magnetohydrodynamic dynamo: Convection in a rotating spherical shell, *Phys. Fluids B*, *5*, 2793–2805.
 - [26] Kageyama, A., T. Sato, K. Watanabe, R. Horiuchi, T. Hayashi, Y. Todo, T. Watanabe, and H. Takamaru (1995), Computer simulation of a magnetohydrodynamic dynamo. II, *Phys. Plasmas*, *2*, 1421–1431.

- [27] Kageyama, A., M. M. Ochi, and T. Sato (1999), Flip-flop transitions of the magnetic intensity and polarity reversals in the magnetohydrodynamic dynamo, *Phys. Rev. Lett.*, *82*, 5409–5412.
- [28] Kuang, W., and J. Bloxham (1999), Numerical modeling of magnetohydrodynamic convection in a rapidly rotating spherical shell: Weak and strong field dynamo action, *J. Comput. Phys.*, *153*, 51–81.
- [29] Li, J., T. Sato, and A. Kageyama (2002), Repeated and sudden reversals of the dipole field generated by a spherical dynamo action, *Science*, *295*, 1887–1890.
- [30] Machetel, P., M. Rabinowicz, and P. Bernardet (1986), Three-dimensional convection in spherical shells, *Geophys. Astrophys. Fluid Dyn.*, *37*, 57–84.
- [31] Matsui, H., and H. Okuda (2002), Development of a simulation code for MHD dynamo processes using the geofem platform, *Inter. J. Comput. Fluid Dyn.*, in press.
- [32] Meakin, R. L. (1992), Computations of the unsteady flow about a generic wing/pylon/finned-store configurations, *AIAA, 92-4568-CP*, 564–580.
- [33] Meakin, R. L. (1993), Moving body overset grid methods for complete aircraft tiltrotor simulations, *AIAA, 93-3350-CP*, 576–588.
- [34] Ochi, M. M., A. Kageyama, and T. Sato (1999), Dipole and octapole field reversals in a rotating spherical shell: Magnetohydrodynamic dynamo simulation, *Physics of Plasmas*, *6*, 777–787.
- [35] Phillips, N. (1957), A map projection system suitable for large-scale numerical weather prediction, *J. Meteor. Soc. Japan, 75th Anniversary Volume*, 262–267.
- [36] Phillips, N. A. (1959), Numerical integration of the primitive equations on the hemisphere, *Month. Weather Rev.*, *87*, 333–345.
- [37] Rai, M. M. (1986), A conservative treatment of zonal boundaries for Euler equation calculations, *J. Comput. Phys.*, *62*, 472–503.
- [38] Ratcliff, J., G. Schubert, and A. Zebib (1996), Steady tetrahedral and cubic patterns of spherical shell convection with temperature-dependent viscosity, *J. Geophys. Res.*, *101*, 25,473–25,484.
- [39] Richards, M. A., W.-S. Yang, J. R. Baumgardner, and H.-P. Bunge (2001), Role of a low-viscosity zone in stabilizing plate tectonics: Implications for comparative terrestrial planetology, *Geochem. Geophys. Geosyst.*, *2*(8), doi:10.1029/2000GC000115.
- [40] Rogers, S. E., H. V. Cao, and T. Y. Su (1998), Grid generation for complex high-lift configurations, *AIAA, 98-3011*, 1–11.
- [41] Ronchi, C., R. Iacono, and P. S. Paolucci (1996), The “cubed sphere”: A new method for the solution of partial differential equations in spherical geometry, *J. Comput. Phys.*, *124*, 93–114.
- [42] Sakuraba, A., and M. Kono (1999), Effect of the inner core on the numerical solution of the magnetohydrodynamic dynamo, *Phys. Earth Planet. Inter.*, *111*, 105–121.
- [43] Steger, J. L. (1982), On application of body conforming curvilinear grids for finite difference solution of external flow, in *Numerical Grid Generation*, J.F. Thomposon, ed., North-Holland, New York, 295–316.
- [44] Steger, J. L., F. C. Dougherty, and J. A. Benek (1983), A chimera grid scheme, *Advances in Grid Generation*, edited by K.N. Ghia and U. Ghia, 59–69.
- [45] Tabata, M., and A. Suzuki (2000), A stabilized finite element method for the rayleigh-benard equations with infinite Prandtl number in a spherical shell, *Comp. Meth. Appl. Mech. Engrg.*, *190*, 387–402.
- [46] Takahashi, F., J. S. Katayama, M. Matsushima, and Y. Honkura (2001), Effects of boundary layers on magnetic field behavior in an MHD dynamo model, *Phys. Earth Planet. Inter.*, *128*, 149–161.
- [47] Tilgner, A. (1999), Spectral methods for the simulation of incompressible flow in spherical shells, *Int. J. Num. Meth. Fluids*, *30*, 713–724.
- [48] Yoshida, M., and A. Kageyama (2004), Application of the yin-yang grid to a thermal convection of a Boussinesq fluid with infinite Prandtl number in a three-dimensional spherical shell, *Geophys. Res. Lett.*, submitted.
- [49] Zhang, S., and D. A. Yuen (1995), The influences of lower mantle viscosity stratification on 3D spherical-shell mantle convection, *Earth Planet. Sci. Lett.*, *132*, 157–166.
- [50] Zhong, S., M. T. Zuber, L. Moresi, and M. Gurnis (2000), Role of temperature-dependent viscosity and surface plates in spherical shell models of mantle convection, *J. Geophys. Res.*, *105*, 11,063–11,082.

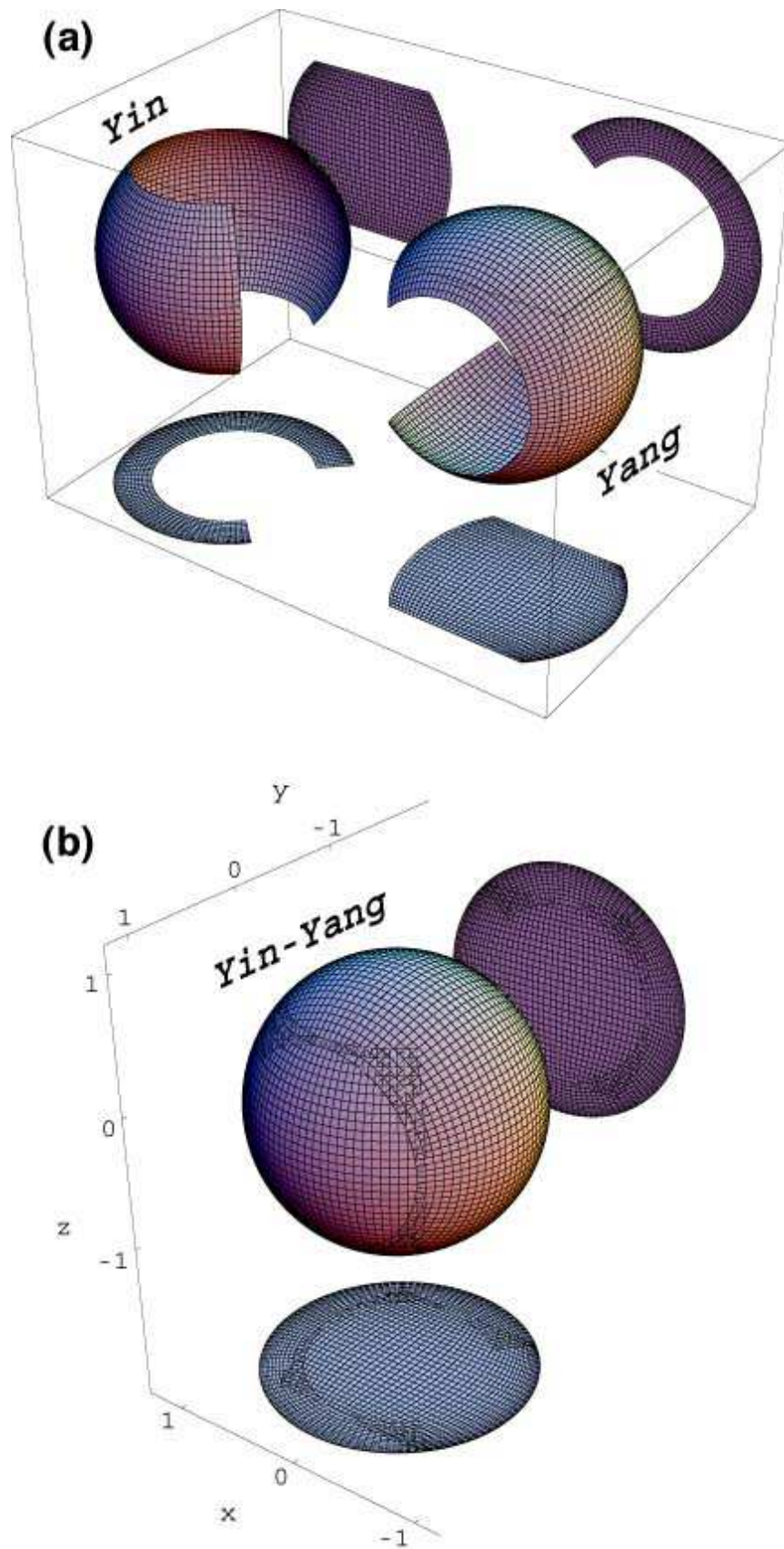


FIG. 1: Basic Yin-Yang grid. (a) It is a spherical overset grid composed of two identical component grids, named Yin and Yang. (b) The Yin grid and Yang grid are combined to cover a spherical surface with partial overlap.

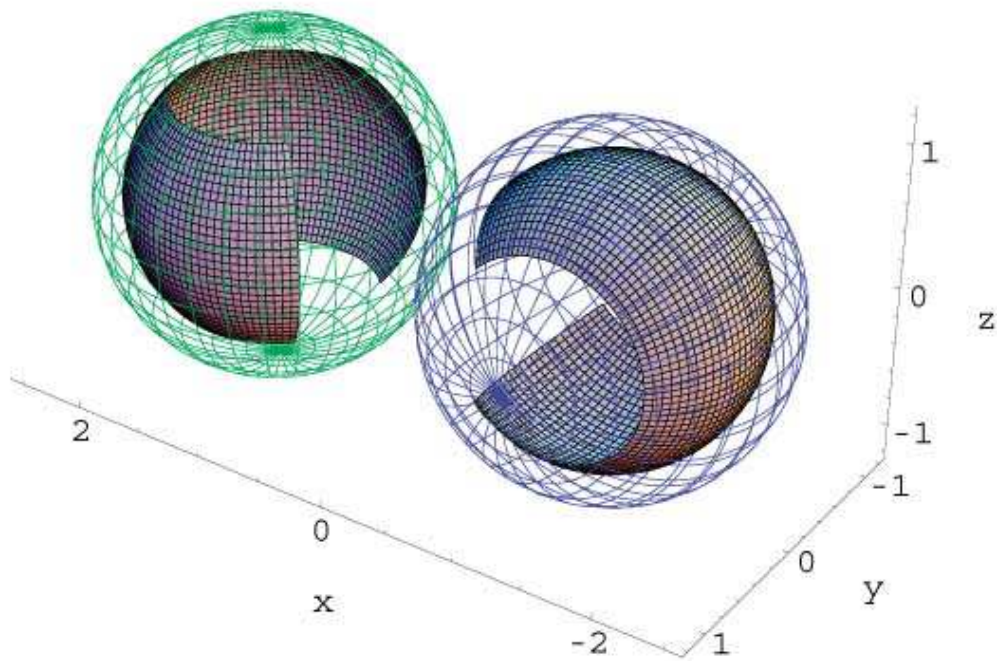


FIG. 2: The component grid of the Yin-Yang grid is a part of the latitude-longitude grid. The axes of two spherical polar coordinates for Yin grid (green mesh) and Yang grid (blue mesh) are perpendicular.

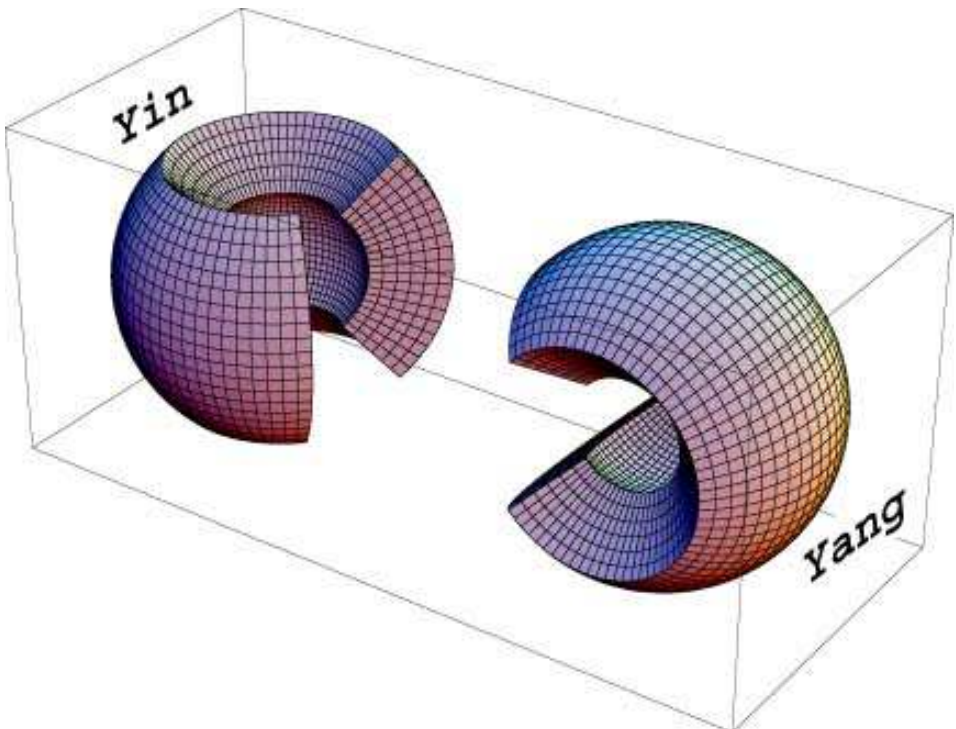


FIG. 3: Three-dimensional Yin-Yang grid for spherical shell geometry. This is constructed by piling up the basic Yin-Yang grid shown in Fig. 1 in the radial direction.

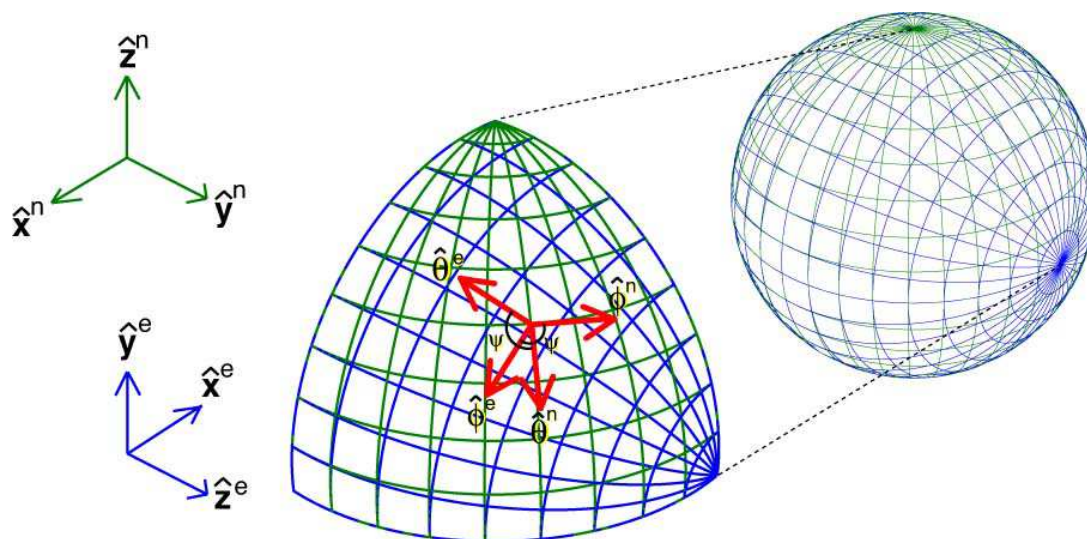


FIG. 4: Unit horizontal vectors of Yin and Yang coordinates. They are mapped one another by a local rotation transform with angle ψ .

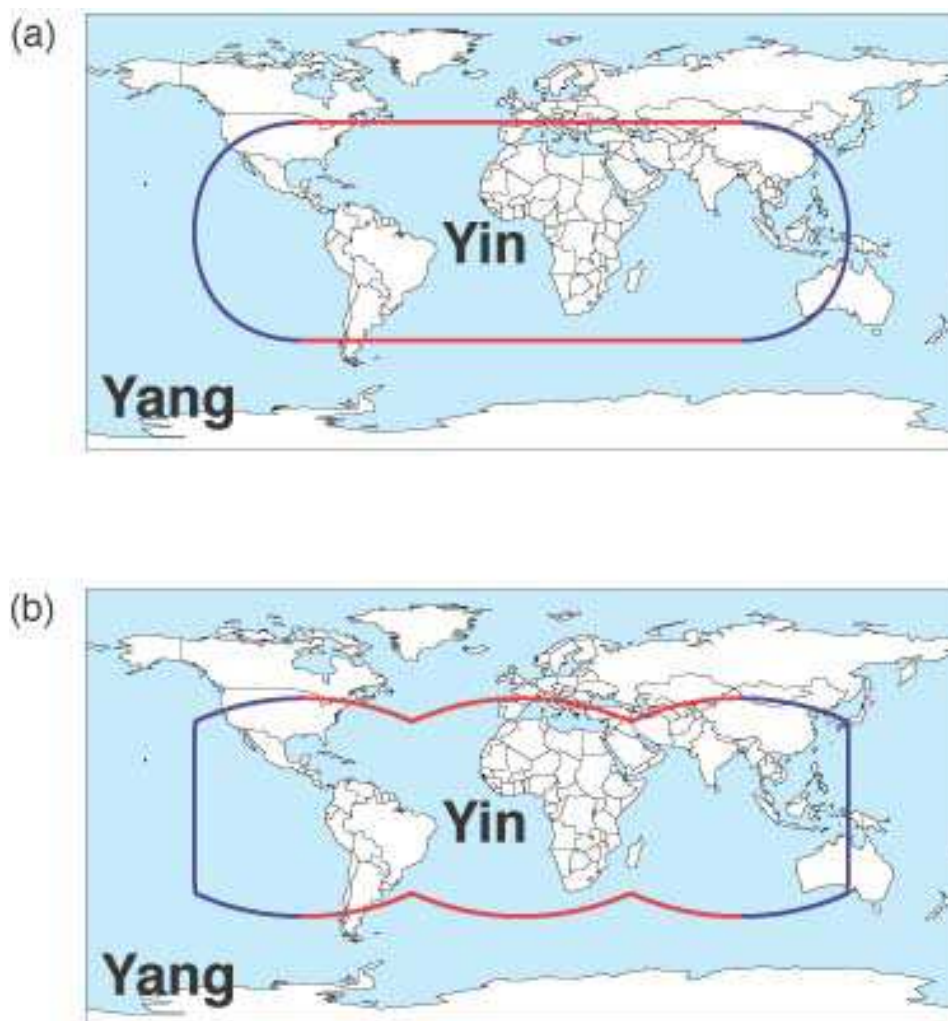


FIG. 5: Curves that divide a spherical surface into two identical areas. If one cuts along the blue-red curve of the panel (a) or (b), the spherical surface is divided into two parts (denoted by Yin and Yang in the pictures) that are exactly the same shape and size. The blue part of the curve and red part of the curve are in the complementary relation; The blue curve of Yin is red curve of Yang, and vice versa.

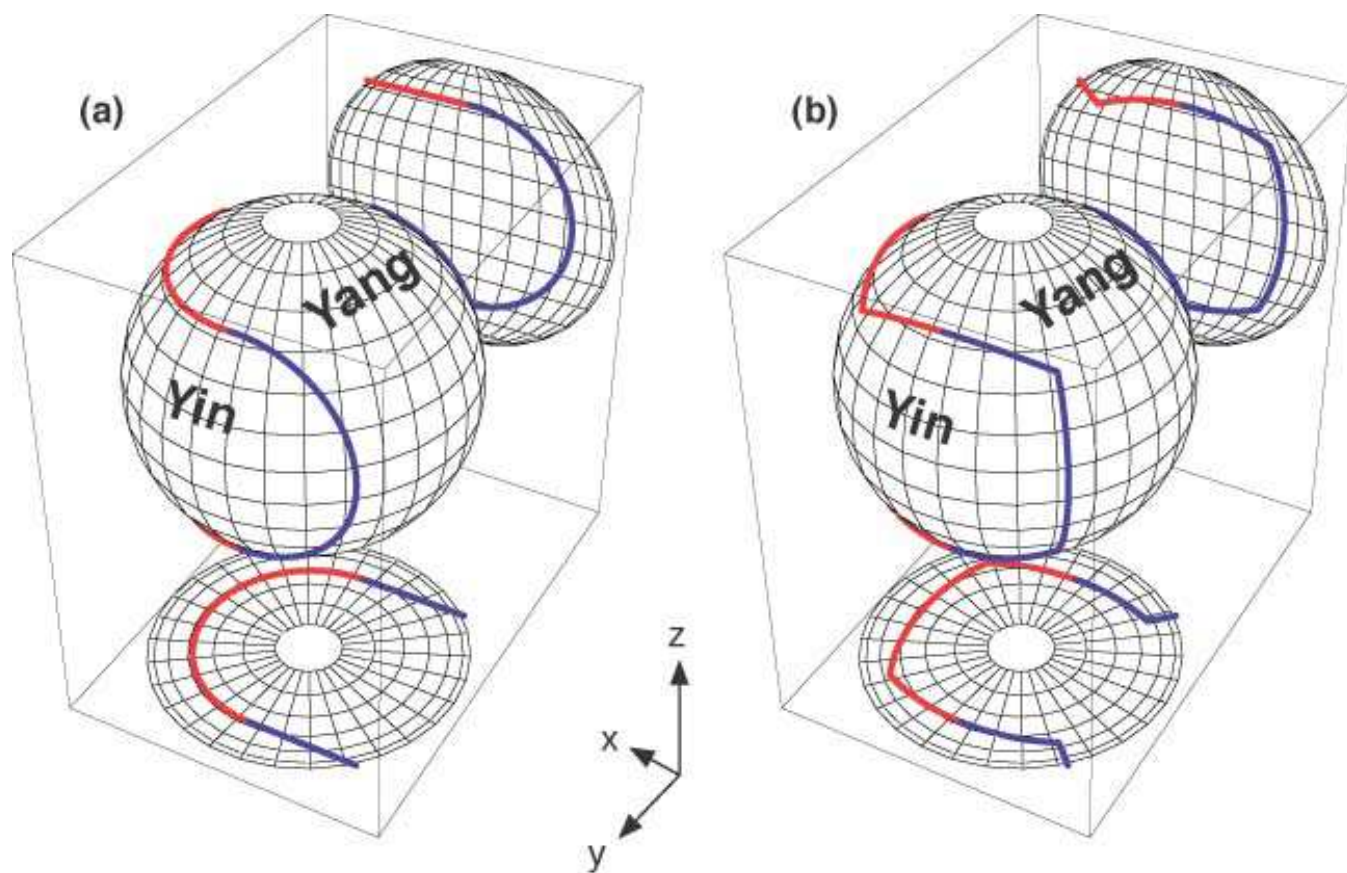


FIG. 6: Curves that divide a spherical surface into two identical areas. These are corresponding three-dimensional views of the red-blue curves in (a) and (b) of Fig. 5.

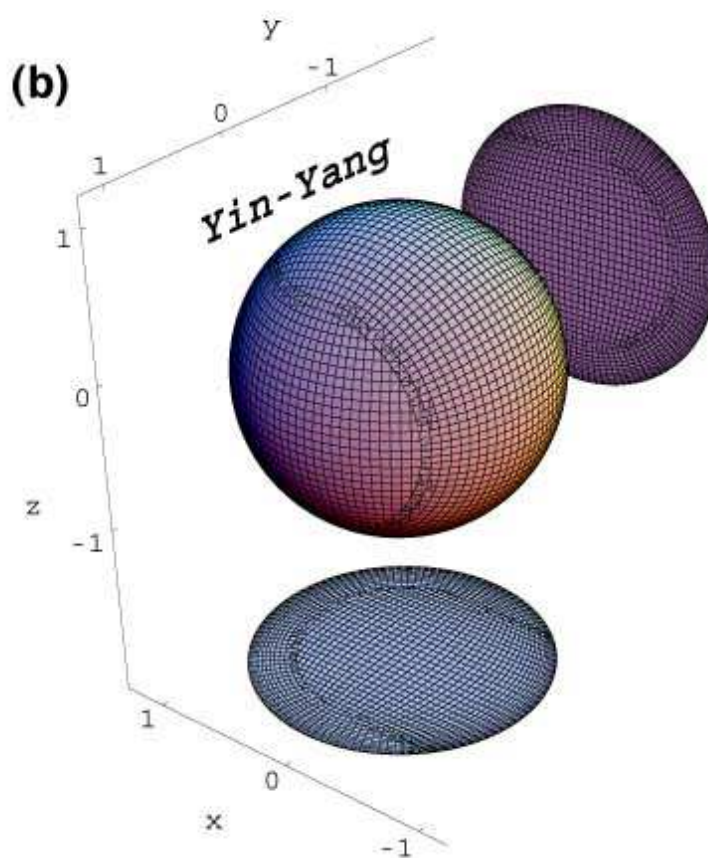
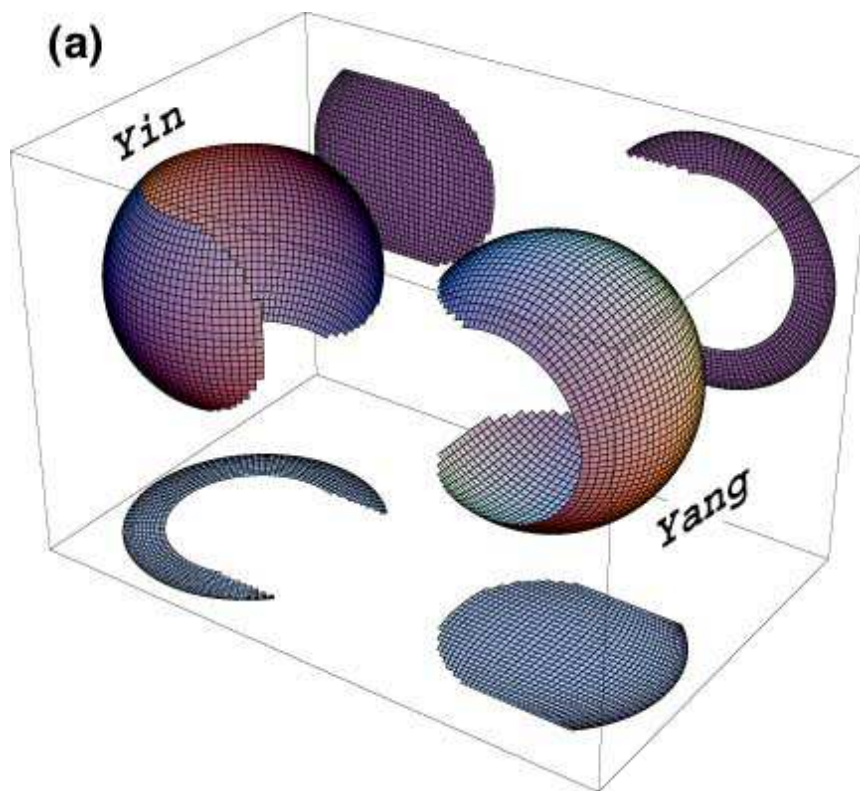


FIG. 7: A Yin-Yang grid with minimum overlap that has the baseball-like border curve between Yin and Yang grids. Corresponding spherical dissection is Figs. 5(a) and 6(a).

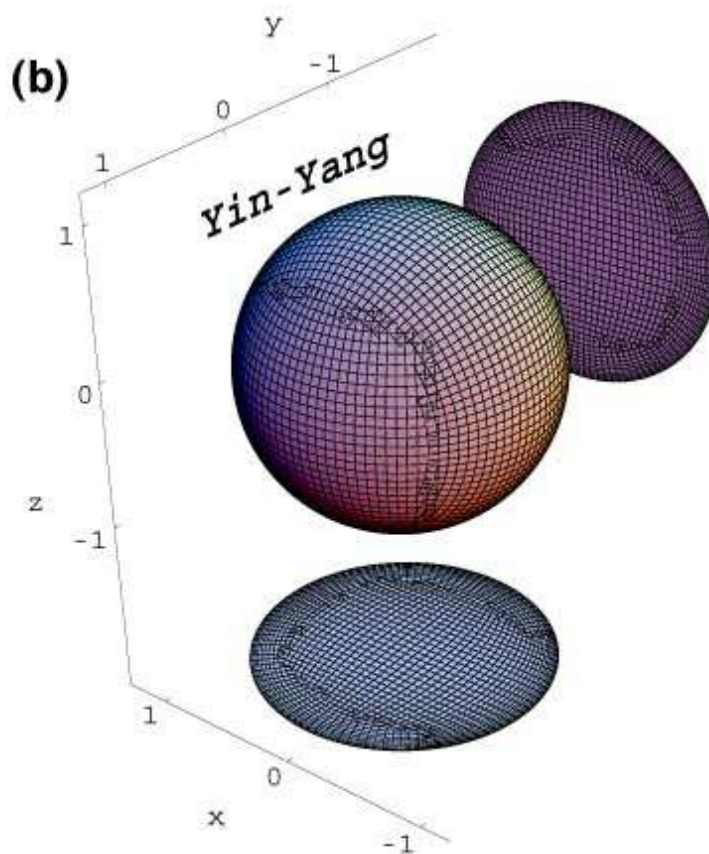
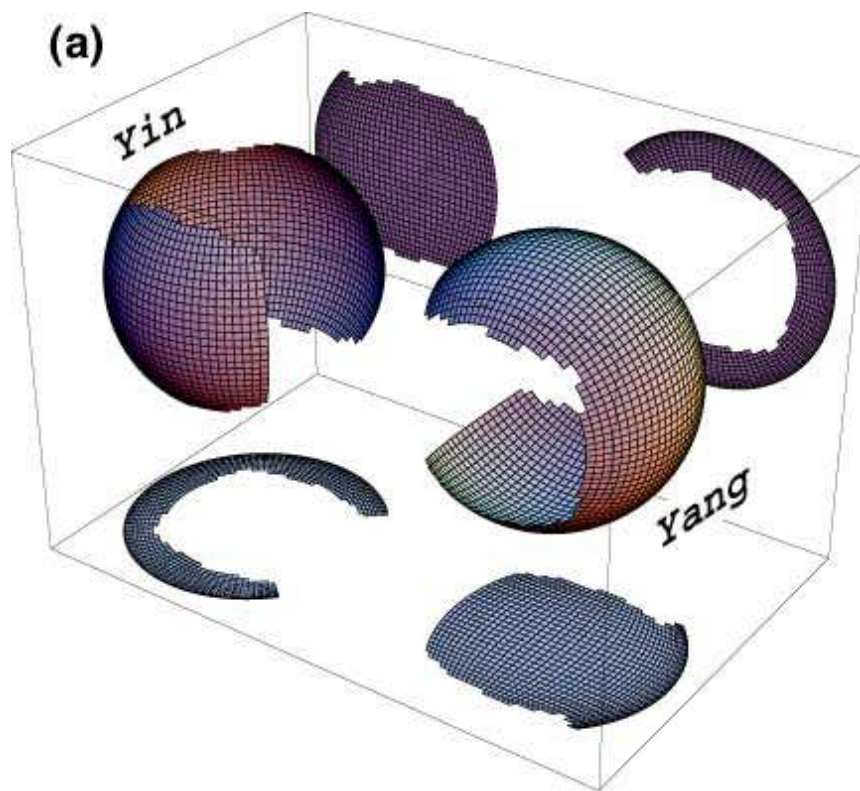


FIG. 8: Another Yin-Yang grid with minimum overlap. The border curve between Yin and Yang grids is cube-like. Corresponding spherical dissection is Figs. 5(b) and 6(b).

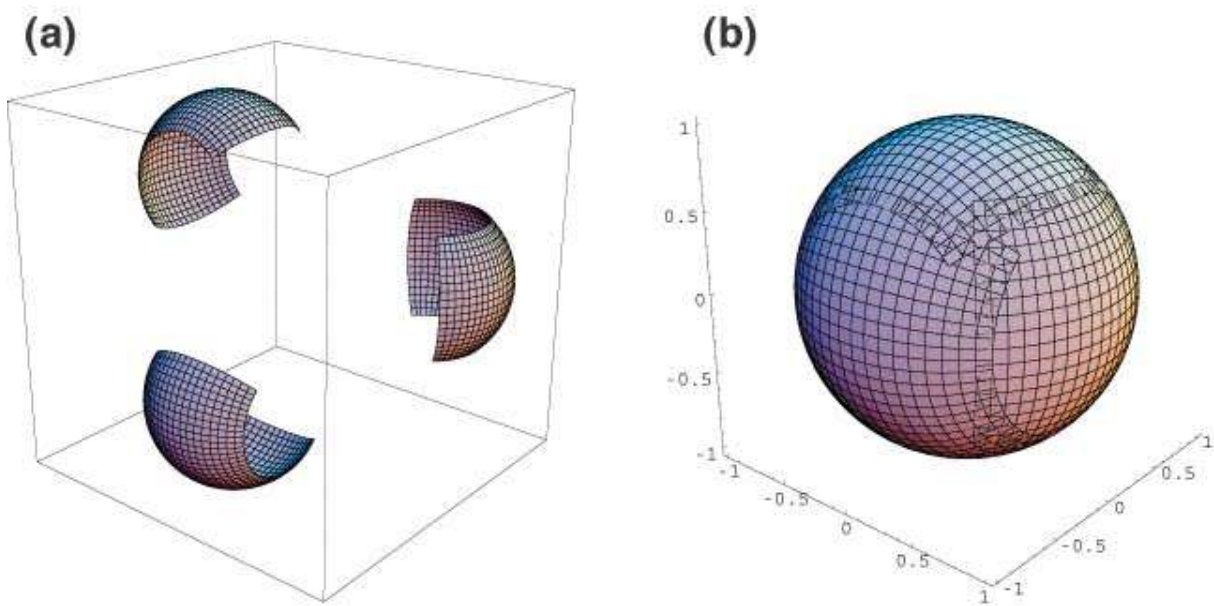


FIG. 9: Another possible spherical overset grid that is composed of three identical component grids.